Dynamics of a driven single flux line in superconductors

Colin Denniston
Department of Physics, Princeton University, Princeton, New Jersey 08544

Chao Tang
NEC Research Institute, 4 Independence Way, Princeton, New Jersey 08540
(Received 27 July 1994)

We study the low-temperature dynamics of a single flux line in a bulk type-II superconductor, driven by a surface current, both near and above the onset of an instability which sets in at a critical driving. We found that above the critical driving, the velocity profile of the flux line develops a discontinuity.

The dynamics of a driven elastic string have attracted much recent attention.[1,2] While most of the work has been focused on the interesting physics of pinning-depinning transitions in the case of bulk driving, a paper by Tang, Feng, and Golubovic[2] studied the case of a surface-current-driven flux line in a bulk type-II superconductor. They found a novel instability of the flux line motion at large driving currents. The instability sets in at a critical driving, where the line loses its steady state motion and (presumably) will be stretched longer and longer. Their finding depends crucially on the boundary condition they use. Physically, the surface driving current is within a boundary layer of thickness λ, where λ is the penetration depth. The boundary condition used in Ref. 2 is somewhat equivalent to taking the limit $\lambda \to 0$ in a plausible but uncontrolled way. Since the instability sets in at or near the boundaries, it is necessary to examine the situation carefully using a more physical boundary layer. Also, it is important to see what happens when the driving current is larger than the critical driving—a question which cannot be addressed by using the boundary condition in Ref. 2.

In this paper we analyze the flux motion with the more physical boundary layer Lorentz driving force. We first use the method of matching asymptotic expansions to study the steady state solutions. The lowest-order matching condition justifies the form of the boundary conditions used in Ref. 2 and gives the relation of the driving force to the current. We then study, both numerically and analytically, the complete equation below and *above* the onset of instability.

Let us first derive the equation for the flux line motion which involves the Lorentz force as a term in the equation, as opposed to just a boundary condition. As we will be mostly interested in fairly large driving forces, we neglect pinning effects. The Lorentz force on a flux line is just $\mathbf{F} = \frac{1}{c}\int \mathbf{j} \times \mathbf{h} ds dA$, where s is the arclength along the flux line and dA a section of infinitesimal area transverse to the flux line. If the applied current $\mathbf{j}$ is slowly varying in the direction *transverse* to the line, then the integration in these coordinates may be carried out to give

$$\mathbf{F} = \frac{\phi_0}{c}\int \mathbf{j} \times \mathbf{t} ds, \tag{1}$$

where ϕ_0 is the flux quantum and $\mathbf{t}$ is the unit tangent vector in the direction of the local magnetic field (the arclength is taken to be increasing in the direction of the magnetic field). The exact form of the current depends on the geometry of the sample; however, it is known that the magnitude of the applied current drops exponentially with distance from the boundary of the sample.

For simplicity we model the dynamics of a single flux line as a two-dimensional problem, defined by its shape function $\mathbf{r}(s,t)$, or where the parametrization is well defined, $y(x,t)$ (see Fig. 1). The applied field is in the negative x direction, and the applied current in the negative z direction, thus giving the driving Lorentz force predominantly in the y direction. The Lorentz force *per unit length* is then

$$\frac{d\mathbf{F}}{ds} = \frac{\phi_0}{c} j_0 \left\{ \exp\left(\frac{x - L/2}{\lambda}\right) + \exp\left(\frac{-x - L/2}{\lambda}\right) \right\} \mathbf{n}, \tag{2}$$

where j_0 is the current density at the surface, the sample boundary is at $x = \pm L/2$, and $\mathbf{n} = -\hat{\mathbf{z}} \times \mathbf{t}$ is the local unit normal vector of the flux line.

The equation of motion for the flux line becomes

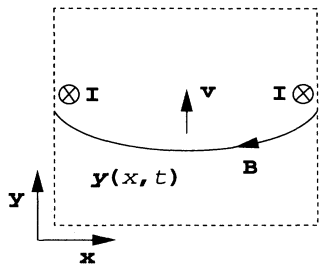

FIG. 1. Sketch of the cross section of the sample. The driving current I is near the sample surfaces. The direction of the magnetic field $\mathbf{B}$ and the direction of the general motion of the line $\mathbf{v}$ are also indicated.

0163-1829/95/51(13)/8457(5)/$06.00 ©1995 The American Physical Society

$$\gamma\dot{\mathbf{r}} = \left[\sigma K + \frac{\phi_0}{c} j_0 \left\{ \exp\left(\frac{x - L/2}{\lambda}\right) + \exp\left(\frac{-x - L/2}{\lambda}\right)\right\}\right]\mathbf{n}. \tag{3}$$

The left-hand side, the viscous damping, and the first term on the right, the normal force due to line tension, are the same as in Ref. 2, and the last term is the Lorentz force, from Eq. (2). γ is the damping coefficient ($\gamma \approx \frac{\phi_0^2}{2\pi\xi^2 c^2 \rho_n}$ from the Bardeen-Stephen model,[3] with ξ the coherence length and ρ_n the normal state resistivity), and σ is the line tension, given approximately by $\frac{H_c^2}{8\pi} 4\pi\xi^2 \ln(\kappa)$, with H_c the critical field and $\kappa \equiv \lambda/\xi$ the Ginzburg-Landau parameter. K is the curvature, and we have the relations $\mathbf{t} = \partial_s \mathbf{r}$ and $\partial_s \mathbf{t} = K\mathbf{n}$.

In cases where the tangent vector never becomes vertical (i.e., $\partial y/\partial x$ remains finite), Eq. (3) can be rewritten in terms of the x and y coordinates of $\mathbf{r}$, now reparametrized by x. Note that a displacement of Δn in the direction of the normal is related to a displacement $\Delta y = \Delta n\sqrt{1 + (\partial y/\partial x)^2}$ and the curvature in terms of x and y is given by $K = [1 + (\partial y/\partial x)^2]^{-3/2}(\partial^2 y/\partial x^2)$. Thus we get the equation

$$\frac{\gamma \frac{\partial y}{\partial t}}{\sqrt{1 + (\frac{\partial y}{\partial x})^2}} = \frac{\sigma \frac{\partial^2 y}{\partial x^2}}{\left[1 + (\frac{\partial y}{\partial x})^2\right]^{\frac{3}{2}}} + \frac{\phi_0 j_0}{c}\left[\exp\left(\frac{x - L/2}{\lambda}\right) + \exp\left(\frac{-x - L/2}{\lambda}\right)\right]. \tag{4}$$

We now examine the *steady state* solutions of Eq. (4). Steady state implies $v = \partial y/\partial t$ is constant, which allows us to rewrite (4) as a first-order equation in the sine of the tangent angle θ. Setting $f = \frac{\phi_0 j_0 \lambda}{c\sigma}$ and $w = \sin\theta = \frac{\partial y}{\partial x}/\sqrt{1 + (\partial y/\partial x)^2}$ we get

$$\lambda \frac{\partial w}{\partial x} = \left(\frac{\gamma}{\sigma} v\right)\lambda\sqrt{1 - w^2} - f\left[\exp\left(\frac{x - L/2}{\lambda}\right) + \exp\left(\frac{-x - L/2}{\lambda}\right)\right]. \tag{5}$$

For x far from the boundaries (i.e., $|x \pm L/2| \gg \lambda$) the driving term is negligible and the equation becomes

$$\frac{\partial w_o}{\partial x} = \left(\frac{\gamma}{\sigma} v\right)\sqrt{1 - w_o^2}. \tag{6}$$

which has solution

$$w_o = \sin\left(\frac{\gamma}{\sigma} v x\right). \tag{7}$$

Now we examine the solution near the boundary at $x = L/2$. The coordinate appropriate in this region is $\eta = -\frac{x - L/2}{\lambda}$. In terms of η, our Eq. (5) becomes

$$\frac{\partial w_i}{\partial \eta} = -\left(\frac{\gamma}{\sigma} v\right)\lambda\sqrt{1 - w_i^2} + f e^{-\eta}. \tag{8}$$

If we expand w_i in powers of $\left(\frac{\gamma}{\sigma} v\right)\lambda$ as $w_i = w_i^{(0)} + \left(\frac{\gamma}{\sigma} v\right)\lambda w_i^{(1)} + \cdots$, we obtain a series of equations for the $w_i^{(n)}$. The first two of these equations are

$$\begin{aligned} \frac{\partial w_i^{(0)}}{\partial \eta} &= f e^{-\eta}, \\ \frac{\partial w_i^{(1)}}{\partial \eta} &= -\sqrt{1 - (w_i^{(0)})^2}. \end{aligned} \tag{9}$$

Assuming an applied field perpendicular to the boundary, these have the solution

$$\begin{aligned} w_i^{(0)} &= f(1 - e^{-\eta}), \\ w_i^{(1)} &= \sqrt{1 - f^2(1 - e^{-\eta})^2} - 1 - f \arcsin f(1 - e^{-\eta}) \\ &\quad -\sqrt{1 - f^2}\left\{\ln\frac{1 - f^2(1 - e^{-\eta}) + \sqrt{(1 - f^2)[1 - f^2(1 - e^{-\eta})^2]}}{1 + \sqrt{1 - f^2}} + \eta\right\}. \end{aligned} \tag{10}$$

If we expand w_o about $x = L/2$ ($\eta = 0$) and w_i for large η, we get

$$w_o \longrightarrow \sin\left(\frac{\gamma v L}{2\sigma}\right) - \left(\frac{\gamma v \lambda}{\sigma}\right)\cos\left(\frac{\gamma v L}{2\sigma}\right)\eta + \cdots,$$

$$w_i \longrightarrow f + \left(\frac{\gamma v \lambda}{\sigma}\right)\left\{\sqrt{1-f^2}\left[1 - \ln\frac{2(1-f^2)}{1+\sqrt{1-f^2}}\right] - 1 - f\arcsin f\right\} - \sqrt{1-f^2}\quad \eta. \tag{11}$$

Matching w_o to w_i gives, to order $\frac{\gamma v \lambda}{\sigma}$,

$$v = \frac{2\sigma}{L\gamma}\arcsin\left[f + \left(\frac{\gamma v \lambda}{\sigma}\right)\left\{\sqrt{1-f^2}\left[1 - \ln\frac{2(1-f^2)}{1+\sqrt{1-f^2}}\right] - 1 - f\arcsin f\right\}\right] \quad (f \le 1). \tag{12}$$

Note that the velocity found in Ref. 2 is obtained by dropping the term of order $\frac{\gamma v \lambda}{\sigma}$ on the right-hand side of (12) and thus is the zeroth order of our asymptotic solution. This matching procedure is illustrated in Fig. 2(b) which shows $w = \sin\theta$ as a function of x for $f = 0.9$. The solid line is a steady state numerical solution, and the dot-dashed and dashed lines show the inner and outer solutions, respectively. We see that the outer and inner solutions agree very well with the numerical result within their respective domains of validity. A composite solution, valid on the whole domain, can be formed by adding w_o and w_i and subtracting their common part from Eq. (11). This is indistinguishable from the numerical solution in Fig. 2(b).

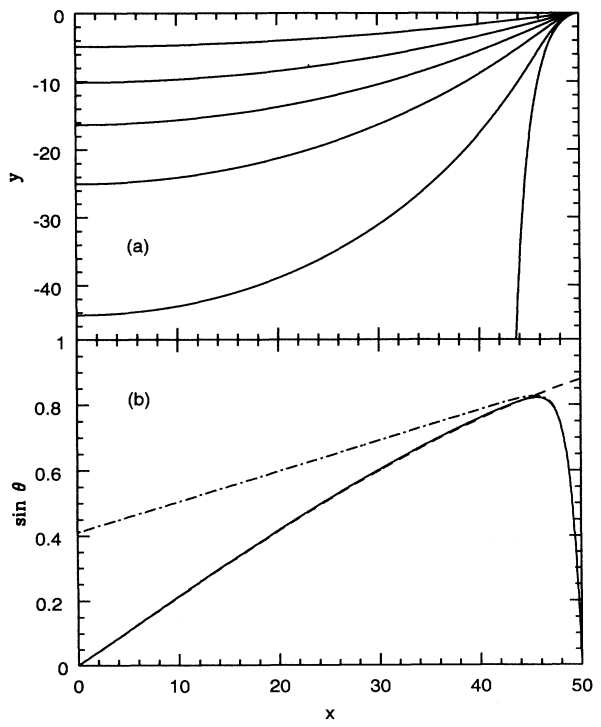

FIG. 2. (a) Steady state flux line profiles for, from top to bottom, f=0.2, 0.4, 0.6, 0.8, 1.0, and 1.1. (b) Matched asymptotic expansions for $f = 0.9$: numerical solution (solid line), w_o (dashed line), and w_i (dot-dashed line).

The numerical solutions shown in Fig. 2 were produced from solutions of Eq. (3). This was chosen, rather than Eq. (4), in x-y coordinates, due to problems arising in the continuity of $\partial y/\partial t$ and the diverging values of $\partial y/\partial x$ found at large values of f (see below). As our equation involves the position vector $\mathbf{r}$ explicitly, we must evolve a set of vectors $\{\mathbf{r}(s)\}$ of positions along the curve (as opposed to, for instance, following the curvature). We solve Eq. (3) using a finite-difference approach. The viscous term $\gamma\dot{\mathbf{r}}$ and the curvature term $K\mathbf{n} = \mathbf{r}_{ss}$ can be dealt with using a Crank-Nicholson-type approach for diffusive equations. This yields two, x and y, tridiagonal systems linked only at the boundaries. The Lorentz force in (3) is then dealt with in a semi-implicit manner. The system is remeshed at each time step to preserve point spacing in regions of high curvature.

For a specific case, we take a sample width L of 100λ and measure the velocity in the unit of σ/γ. Figure 2(a) shows the line shapes for $f = 0.2$–1.1. We see that the slope remains fairly small within a penetration depth λ of the boundary, consistent with the assumptions for Eq. (1). Also, the analytic solution of Ref. 2 starts to deviate from our numerical solution near the boundary for large f.

Figure 3 shows v as a function of f. The crosses are from steady state numerical solutions, the dashed line is the zeroth-order matching condition from Ref. 2, and the dotted line (for the region $f \le 1$) is from Eq. (12). The zeroth-order solution suggests that as $f \to 1$, $v \to v_{\max} = \pi\sigma/\gamma L$, implying $\theta \to \pi/2$; i.e., the flux line "wets" the boundary. The more accurate expression, Eq. (12), suggests that $v \to \frac{2\sigma}{L\gamma}\arcsin[1 - (\frac{\gamma v\lambda}{\sigma})(1+\pi/2)] < v_{\max}$, and so the flux line does not become vertical as $f \to 1$ (see also the numerical solution in Fig. 2). What then does happen for f greater than 1? As we shall see below, the flux line becomes vertical ($\theta \to \pi/2$) at an interior point, but not until $f = f^* = 1.076\,23$ for our sample case where $\lambda/L = 0.01$. Above f^* the speed of the flux line develops a discontinuity, becoming piecewise constant.

Note that in the above analysis $w_i^{(0)} > 1$ for $f > 1$, and so it cannot be extended to the region where $f > 1$. This problem can be remedied by adjusting the arbitrary constant in $w_i^{(0)}$ so that $w_i^{(0)}$ does not exceed 1. This means that $w_i^{(0)}$ will no longer satisfy the boundary con-

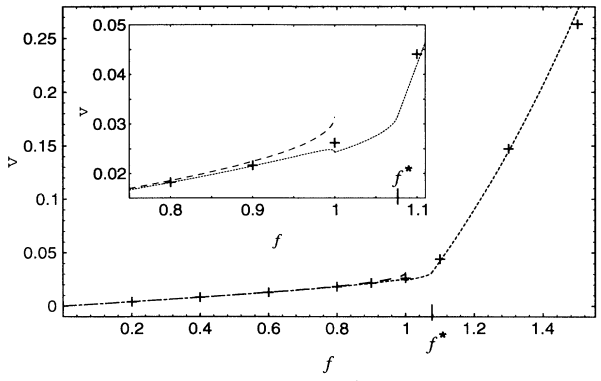

FIG. 3. The velocity of the flux line as a function of driving force: numerical simulations (crosses), Eqs. (12), (15), and (16) (dotted line), and Eq. (10) of Ref. 1 which is also the zeroth order of Eq. (12) (dashed line). Inset: a blowup of the figure near $f = 1$.

dition $w_i^{(0)}|_{\eta=0} = 0$. We can, however, adjust the constant in $w_i^{(1)}$ to compensate for this discrepancy so that $w_i^{(0)} + (\frac{\gamma v\lambda}{\sigma})w_i^{(1)} = 0$ at $\eta = 0$. This results in a solution to Eq. (9), for $f > 1$, of

$$w_i^{(0)} = 1 - fe^{-\eta},$$
$$w_i^{(1)} = \left(\frac{\sigma}{\gamma v\lambda}\right)(f-1) + \sqrt{\frac{2}{f}e^{-\eta} - e^{-2\eta}} - \sqrt{\frac{2}{f} - 1} + 2\arcsin\sqrt{\frac{e^{-\eta}}{2f}} - 2\arcsin\sqrt{\frac{1}{2f}}. \quad (13)$$

Expanding this w_i for large η gives

$$w_i \longrightarrow f - \left(\frac{\gamma v\lambda}{\sigma}\right)\left[\sqrt{\frac{2}{f} - 1} + 2\arcsin\sqrt{\frac{1}{2f}}\right]. \quad (14)$$

Matching this to w_o at $x = L/2$ gives, to order $\frac{\gamma v\lambda}{\sigma}$,

$$v = \frac{2\sigma}{L\gamma}\arcsin\left[f - \left(\frac{\gamma v\lambda}{\sigma}\right) \times \left\{\sqrt{\frac{2}{f} - 1} + 2\arcsin\sqrt{\frac{1}{2f}}\right\}\right]. \quad (15)$$

Note that for $f = 1$, $v = \frac{2\sigma}{L\gamma}\arcsin[f - (\frac{\gamma v\lambda}{\sigma})(1+\pi/2)]$, the same result as taking $f \to 1$ in Eq. (12). Equation (15) has only real solutions for $f \leq f^* = 1.076\,23$ (for $L = 100\lambda$). It suggests that the instability should occur at $f = f^*$ where $v = v_{\max} = \pi\sigma/\gamma L$. Equation (15) is shown as the continuation of the dotted line for $1 < f < f^*$ in Fig. 3. For general λ/L, f^* is found as the root of Eq. (15) for $v = v_{\max} = \pi\sigma/\gamma L$. For small λ/L, the case we are interested in, this root is

$$f^* \approx 1 + \frac{\lambda}{L}(\pi + \pi^2/4). \quad (16)$$

We see that as $\lambda/L \to 0$, $f^* \to 1$.

The question now arises as to what happens above f^*. Figure 4(a) shows the numerical evolution of the flux line shape for $f = 1.1$, just above the transition, and $f = 1.5$. There are two important things to note in this figure. First, the flux line is approaching a vertical asymptote at about $x = 40.5$ in what seems to be an asymptotic manner (i.e., the flux line does not become vertical in a finite amount of time). Second, the portion of the flux line to the boundary side of this vertical asymptote has a constant shape, implying *it is moving with a constant speed in the y direction.* This last observation can be verified by applying a finite-difference approximation to Eq. (4) to compute $\partial y/\partial t$ for the points on the flux lines of Fig. 4(a). The result of this computation is shown in Fig. 4(b). We see from this velocity profile that, indeed, the speed is constant in the boundary layer, but that a *discontinuity* has developed in the velocity profile. The constant speed of the boundary layer can be deduced as follows.

Equation (14) gives the *constant* asymptotic value of w_i for large η. Above f^* this asymptotic value can only be 1 ($w_i = \sin\theta \leq 1$), as the flux line becomes vertical. So setting (14) to one gives the speed of the inner solution, v_i, for $f > f^*$ as

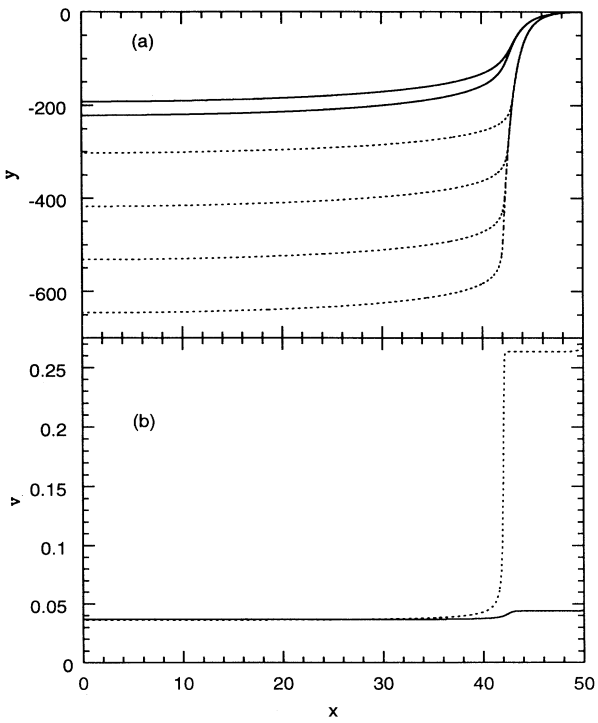

FIG. 4. (a) The shape of the flux line at different times for $f = 1.1$ (solid lines) and $f = 1.5$ (dotted lines). The solutions which extend further down the plot are at later times. (b) Velocity profiles of the flux lines of (a) at the latest times shown.

$$v_i = \frac{\frac{2\sigma}{\gamma L}(f-1)}{\sqrt{\frac{2}{f}-1}+2\arcsin\sqrt{\frac{1}{2f}}}. \quad (17)$$

This is shown as the dotted line in Fig. 3 for $f > f^*$. Comparison of this speed to the speed obtained in the numerical simulations shows excellent agreement.

Now, what about the outer solution, w_o? We see from Fig. 4 that as time progresses the speed of the outer solution approaches a constant value and that the position of the discontinuity in the velocity profile [or the vertical asymptote in Fig. 4(a)] seems to approach a fixed value. The location of the vertical asymptote and the asymptotic (large time) speed of the inner solution are quite related. Requiring that $w_o \to 1$ at the vertical asymptote gives the speed of the outer solution.

In conclusion, we have studied the flux line motion, in particular the dynamical instability found in Ref. 2, using a more physical boundary layer driving. The boundary condition used in Ref. 2 is consistent with our zeroth-order (in λ) asymptotic matching. The analytic solution of Ref. 2 is quantitatively valid for $f \leq 0.8$. For larger f, the deviations both in line shape near the boundary and in the velocity are significant. We have shown that the instability occurs at $f = f^* = 1 + (\lambda/L)(\pi + \pi^2/4)$ where the flux line starts to lose steady state motion. We have observed numerically that above this instability the flux line velocity profile develops a discontinuity. This instability has a clear mark on the I-V curve, Fig. 3, that is a sharp upward turn at f^*. As pointed out in Ref. 2, this instability should also occur in dense flux line systems.

[1] M. V. Feigel'man, Sov. Phys. JETP **58**, 1076 (1983); R. Bruinsma and G. Aeppli, Phys. Rev. Lett. **52**, 1547 (1984); J. Koplik and H. Levine, Phys. Rev. B **32**, 280 (1985); T. Nattermann, S. Stepanow, L.-H. Tang, and H. Leschhorn, J. Phys. II France **2**, 1483 (1992); G. Parisi, Europhys. Lett. **17**, 673 (1992); K. Sneppen, Phys. Rev. Lett. **69**, 3539 (1992); O. Narayan and D. Fisher, Phys. Rev. B **48**, 7030 (1993); M. Dong, M. C. Marchetti, A. A. Middleton, and V. Vinokur, Phys. Rev. Lett. **70**, 662 (1993); Z. Csahók, K. Honda, E. Somfai, M. Vicsek, and T. Vicsek, Physica A **200**, 136 (1993); H. A. Makse, A.-L. Barabási, and H. E. Stanley (unpublished).

[2] C. Tang, S. Feng, and L. Golubovic, Phys. Rev. Lett. **72**, 1264 (1994).

[3] M. Tinkham, *Introduction to Superconductivity* (McGraw-Hill, New York, 1975), p. 162.